Synchronization and local convergence analysis of networks with dynamic diffusive coupling

Daniel Alberto Burbano Lombana and Mario di Bernardo

Citation: Chaos **26**, 116308 (2016); doi: 10.1063/1.4966017
View online: http://dx.doi.org/10.1063/1.4966017
View Table of Contents: http://aip.scitation.org/toc/cha/26/11
Published by the American Institute of Physics

Synchronization and local convergence analysis of networks with dynamic diffusive coupling

Daniel Alberto Burbano Lombana[a] and Mario di Bernardo[b]
Department of Electrical Engineering and Information Technology, University of Naples Federico II, Naples 8125, Italy

(Received 9 June 2016; accepted 29 September 2016; published online 16 November 2016)

In this paper, we address the problem of achieving synchronization in networks of nonlinear units coupled by dynamic diffusive terms. We present two types of couplings consisting of a static linear term, corresponding to the diffusive coupling, and a dynamic term which can be either the integral or the derivative of the sum of the mismatches between the states of neighbouring agents. The resulting dynamic coupling strategy is a distributed proportional-integral (PI) or a proportional-derivative (PD) law that is shown to be effective in improving the network synchronization performance, for example, when the dynamics at nodes are nonidentical. We assess the stability of the network by extending the classical Master Stability Function approach to the case where the links are dynamic ones of PI/PD type. We validate our approach via a set of representative examples including networks of chaotic Lorenz and networks of nonlinear mechanical systems. *Published by AIP Publishing.* [http://dx.doi.org/10.1063/1.4966017]

The study of the mechanisms and fundamental laws that enable the emergence of complex behaviour in ensembles of cooperative units has become a fundamental problem for science[33] and technology as it is of relevance in many applications.[23] A particular yet important phenomenon often used as a paradigm to investigate the emergence of coordinated behaviour in networks is synchronization.[32] When this happens, the trajectories of all the components of the ensemble asymptotically converge toward each other onto a common solution. Examples include frequency synchronization in power grids, robot vehicle coordination, and even abnormal synchronisation in neural networks.[15,29,44] Typically, the interconnecting links among each component are assumed to be diffusive and static.[25,44] However, this represents a gross oversimplification since in more realistic scenarios the communications links are often of dynamic nature. The aim of this paper is to present a simple yet effective extension of the linear diffusive coupling by making it dynamic via the addition of an integral or a derivative term depending on the mismatch between the states of neighbouring agents. The resulting dynamic coupling strategy is shown to be effective in improving the network synchronization performance.[7]

I. INTRODUCTION

Many natural and engineered systems can be described as ensembles of dynamical systems interacting with each other over a network of interconnections. This approach has been found to be successful for capturing and characterising the behaviour of large and complex systems such as the world-wide-web, metabolic networks, the electrical power grid, and animal groups among many others.[6,42] A particular phenomenon in networks of dynamical systems is synchronisation.[32] When this happens, the trajectories of all the components of the ensemble asymptotically converge toward each other onto a common solution. Synchronization is relevant for different applications ranging from frequency synchronisation in power grids, robot vehicle coordination, and traffic congestion[3,20] to synchronous phenomena observed in Nature as, for instance, in neural networks or flock of birds.[15,29,44] Typically, these multi-agent systems are modelled as networks of dynamical systems interconnected via a static linear diffusive coupling,[15,25,44] and their local stability and convergence are often studied using the Master Stability Function (MSF) approach.[28]

The MSF has been widely accepted for assessing local convergence to synchronisation in this class of networks. The main advantage of the MSF is that it allows to reduce the computational complexity required to assess if synchronization is possible, since instead of studying the stability of the whole network, it is just required to study the stability of one node (master node), which represents all the others in the ensemble.

The MSF approach is a powerful tool for investigating synchronisation in generic networks of identical oscillators, by providing theoretical predictions of such synchronous behaviour. Different extensions and applications of the MSF are available in the literature, for example, an extension of the MSF to the case of nearly identical oscillators has been reported in Ref. 43, while the MSF has also been exploited for studying networks with general delays on the links.[21] Also, the MSF has been used for studying synchronization in hypernetworks[41] and for networks with switching links.[11,22] More recently, the MSF has been used for characterising and predicting the formation of clusters (or patterns) in networks with topological symmetries.[30]

[a]Electronic mail: danielalberto.burbanolombana@unina.it
[b]Electronic mail: mario.dibernardo@unina.it; He is also at Department of Engineering Mathematics, University of Bristol, U.K.

The aim of this paper is twofold: (i) firstly, we present a simple yet effective dynamic extension of linear diffusive coupling that can be used for enhancing synchronisation in networks of identical nonlinear units possibly with parameter mismatches; (ii) secondly, we extend the well-known MSF approach to study local convergence in the case where the links are dynamic of PI/PD type.

To extend the classical diffusive coupling strategy, we add an integral or a derivative term depending on the mismatch between the states of neighbouring agents. The resulting dynamic coupling strategy is a proportional-integral (PI) or a proportional-derivative (PD) law that has been shown to be effective in improving the network synchronization performance.[7] From a control theoretic viewpoint,[34] the approach can be seen as the deployment of distributed PI or PD controllers over a network of interest.[8] The use of PI couplings has been proposed in the literature for achieving consensus in networks of identical nodes with linear dynamics.[2,16] More recently, a distributed PID coupling structure[8] has been proposed for guaranteeing consensus in networks of heterogeneous first order linear agents with constant disturbances. It is important to highlight that distributed PI/PID actions have been also used in different applications comprising synchronization and frequency control in power grids,[5,38,40] clock synchronization in networks of discrete-time integrators in Ref. 10, autonomous space satellites,[2] congestion control,[47] and containment control of mobile robots.[12] Further results still focused on networks of linear agents are reported in Refs. 26, 45, and 46.

Contrary to the previous results in the literature, in this paper, we consider dynamic PI/PD couplings for networks of *nonlinear* possibly chaotic units. The stability of the synchronous solutions is studied by extending the MSF approach to the case where the couplings are dynamic, i.e., PI/PD. Here, the "master node" equations are derived, and the theoretical results are illustrated via a representative example using the networks of chaotic Lorenz systems. Finally, the approach is applied to study synchronization in networks of mechanical nonlinear oscillators. We convincingly show that the dynamic couplings can be properly tuned for enhancing synchronization as well as for decreasing the residual error when some heterogeneities are present at all or some of the nodes. We wish to emphasize that our results can also be useful to investigate synchronization in networks of other nonlinear systems such as those consisting nonlinear circuits[13,14,36] where inductive and capacitive couplings can be modelled as PI/PD coupling.

II. PRELIMINARIES AND PROBLEM FORMULATION

A. Notation

We denote by $\mathbf{I}_N$ the identity matrix of dimension $N\times N$, by $\mathbb{1}_N$ a $N\times 1$ vector with unitary elements. The Frobenius norm is denoted by $\|\cdot\|$. A diagonal matrix, say, $\mathbf{D}$, with diagonal elements $d_1,\ldots,d_N$ is indicated by $\mathbf{D}=\text{diag}\{d_1,\ldots,d_N\}$. The ordered eigenvalues of an $n\times n$ matrix $\mathbf{A}$ with real entries are denoted by λ_1, λ_2, …, λ_n, and $\otimes$ denotes the Kronecker product.[4]

An *undirected graph* $\mathcal{G}$ is defined by $\mathcal{G}=(\mathcal{N},\mathcal{E})$, where $\mathcal{N}=\{1,2,\ldots,N\}$ is the finite set of N node indices, and $\mathcal{E}\subset\mathcal{N}\times\mathcal{N}$ is the set containing the E edges between the nodes $(i,\ j)$ for any $i,j\in\mathcal{N}$. The architecture of the network of interconnections is represented by the *adjacency matrix* $\boldsymbol{\mathcal{A}}\in\mathbb{R}^{N\times N}$ whose entries $\boldsymbol{\mathcal{A}}=[A_{ij}]$ are given by $A_{ij}=1$ if $(i,j)\in\mathcal{E}$ and $A_{ij}=0$ otherwise.

B. Network model

We consider ensembles of N nonlinear units, each one described by a set of nonlinear ordinary differential equations (ODEs) of the form $d\mathbf{x}_i/dt=\mathbf{f}(\mathbf{x}_i)$, where $\mathbf{x}_i\in\mathbb{R}^n$, $\mathbf{f}(\mathbf{x}):\Omega\subseteq\mathbb{R}^n\mapsto\mathbb{R}^n$ is a nonlinear smooth function, and $i\in\{1,\ldots,N\}$. Assuming diffusive coupling among neighbouring units,[25] the overall network dynamics can be written as

$$\frac{d\mathbf{x}_i}{dt}=\mathbf{f}(\mathbf{x}_i)-\sigma\sum_{j=1}^{N}\mathcal{L}_{ij}\mathbf{h}(\mathbf{x}_j,\mathbf{y}_j),\quad \mathbf{x}_i(0)=\mathbf{x}_{i0},i,j\in\mathcal{N},\ (1)$$

where $\mathcal{N}:=\{1,\ldots,N\}$ is the set of indices, while $\mathbf{x}_i(0)=\mathbf{x}_{i0}\in\Omega\subseteq\mathbb{R}^n$, $i\in\mathcal{N}$ are the vectors of initial conditions. The constant and positive scalar σ is the global coupling strength. The function $\mathbf{h}(\mathbf{x}_i,\mathbf{y}_i):\mathbb{R}^n\mapsto\mathbb{R}^n$ represents the coupling between neighbouring units which is characterized by static and dynamic terms via $\mathbf{x}_i$ and $\mathbf{y}_i$, respectively. We consider two particular functional forms for $\mathbf{h}$ (see Section II C), where we assume the dynamic variable $\mathbf{y}_j$ to be $\mathbf{y}_j=\int_0^t\mathbf{x}_j(\tau)d\tau$ or $\mathbf{y}_j=d\mathbf{x}_j/dt$. The network of dynamical units (1) is represented by a graph $\mathcal{G}=(\mathcal{N},\mathcal{E})$, which can be described in terms of its associated Laplacian matrix $\boldsymbol{\mathcal{L}}:=\text{diag}\{\boldsymbol{\mathcal{A}}1_N\}-\boldsymbol{\mathcal{A}}$, where $\boldsymbol{\mathcal{A}}$ is the adjacency matrix representing the topology of the network.

Assumption II.1 *The network of interconnections in (1) represented by a graph $\mathcal{G}=(\mathcal{N},\mathcal{E})$ is assumed to be undirected, unweighted, and connected.*

It is important to highlight that for any connected and undirected graph $\mathcal{G}$, the associated Laplacian matrix $\boldsymbol{\mathcal{L}}$ is a symmetric matrix; therefore, it can be eigen-decomposed[8] as $\boldsymbol{\mathcal{L}}=\mathbf{Q}\boldsymbol{\Lambda}\mathbf{Q}^T$, where $\mathbf{Q}\in\mathbb{R}^{N\times N}$ is an orthonormal matrix given by $\mathbf{Q}:=[\mathbf{q}_1,\ldots,\mathbf{q}_N]$, where $\mathbf{q}_i\in\mathbb{R}^{N\times 1}$ are the eigenvectors of $\boldsymbol{\mathcal{L}}$, and $\boldsymbol{\Lambda}:=\text{diag}\{0,\lambda_2,\ldots,\lambda_N\}$ with $\lambda_i,i\in\mathcal{N}$ being the eigenvalues of $\boldsymbol{\mathcal{L}}$, which can be ordered as $0=\lambda_1<\lambda_2\leq\cdots\leq\lambda_N$.

Here, we are interested in finding necessary and sufficient conditions, guaranteeing that all states $\mathbf{x}_i$ in the network of dynamical units (1) asymptotically converge towards each other, i.e., synchronization.

Definition II.1. *Network (1) is said to reach local synchronisation if there exist a set of initial conditions $\mathbf{x}_i(0)=\mathbf{x}_{i0}\in\Omega\subseteq\mathbb{R}^n$ such that*

$$\lim_{t\to\infty}\|\mathbf{x}_j(t)-\mathbf{x}_i(t)\|=0,\quad i,j\in\mathcal{N}.\ (2)$$

C. Dynamic couplings

Rather than considering the standard static diffusive coupling, we use a control theoretic approach to define two types of dynamic diffusive couplings[8]

- Proportional and Integral (PI)

$$\mathbf{h}(\mathbf{x}_j, \mathbf{y}_j) = \alpha \mathbf{\Gamma}_P \mathbf{x}_j + \beta \mathbf{y}_j, \tag{3}$$

$$\mathbf{y}_i = \mathbf{\Gamma}_I \int_0^t \mathbf{x}_j(\tau) d\tau, \quad i \in \mathcal{N}, \tag{4}$$

where the nodes exchange information on their states using proportional and integral terms. Here, α and β are non-negative constants each representing the strength of the proportional and integral contributions, respectively. The inner coupling matrices $\mathbf{\Gamma}_P, \mathbf{\Gamma}_I \in \mathbb{R}^{n\times n}$ capture the way in which information among nodes is being exchanged by identifying what states a node transmits to its neighbours. For instance, in Example III C, each unit is a third order system where $\mathbf{x} = [x_1, x_2, x_3]^T$. Therefore, setting, for example, $\mathbf{\Gamma}_P = \mathbf{\Gamma}_I = \text{diag}\{1, 0, 0\}$ means that the nodes are solely coupled through the first state variable x_1. Note that, in general, the matrices $\mathbf{\Gamma}_P$ and $\mathbf{\Gamma}_I$ are not necessarily the same, opening the possibility of choosing independently the variables that can be coupled via static or dynamic terms.

The second dynamic coupling we consider is

- Proportional and derivative (PD)

$$\mathbf{h}(\mathbf{x}_j, \mathbf{y}_j) = \alpha \mathbf{\Gamma}_P \mathbf{x}_j + \gamma \mathbf{y}_j, \tag{5}$$

$$\mathbf{y}_i = \mathbf{\Gamma}_D \frac{d\mathbf{x}_j}{dt}, \quad i \in \mathcal{N}, \tag{6}$$

where the nodes exchange information on their states using proportional and derivative terms. Here, α and γ are non-negative constants each representing the strength of the proportional and derivative contributions, respectively, and $\mathbf{\Gamma}_D \in \mathbb{R}^{n\times n}$ is the inner coupling matrix for the derivative term.

III. MASTER STABILITY FUNCTION FOR NETWORKS WITH DYNAMIC COUPLINGS

To study the convergence towards synchronization, we next extend the MSF[28] to networks with dynamic couplings of PI and PD types. For the sake of clarity, we split the analysis in two cases and we derive the master equations for detecting local stable synchronous solutions in network (1).

A. MSF approach for dynamic proportional-integral coupling

Consider network (1) with dynamic PI coupling (3), setting $\mathbf{h}(\cdot) = \mathbf{h}_I$ yields

$$\frac{d\mathbf{x}_i}{dt} = \mathbf{f}(\mathbf{x}_i) - \sigma \sum_{j=1}^{N} \mathcal{L}_{ij} \left(\alpha \mathbf{\Gamma}_P \mathbf{x}_j + \beta \mathbf{y}_j\right), \tag{7}$$

$$\frac{d\mathbf{y}_i}{dt} = \mathbf{\Gamma}_I \mathbf{x}_i, \quad \mathbf{y}_i(0) = 0. \tag{8}$$

From (7) and (8) and from the fact that $\mathcal{L}$ has a zero row-sum, it is immediate to note that the synchronous solution $\mathbf{s} = \mathbf{x}_1 = \cdots = \mathbf{x}_N$ must be such that

$$\frac{d\mathbf{s}}{dt} = \mathbf{f}(\mathbf{s}), \tag{9}$$

$$\frac{d\mathbf{w}}{dt} = \mathbf{\Gamma}_I \mathbf{s}, \tag{10}$$

where $d\mathbf{y}_1/dt = \cdots = d\mathbf{y}_N/dt = d\mathbf{w}/dt$. The master stability function approach studies the local stability of the synchronous solution $\mathbf{s}(t)$, $\mathbf{w}(t)$ in the presence of small perturbations.[28] For the sake of clarity, we split the MSF approach into four steps.

S1: We first assume that the uncoupled dynamical systems (9) and (10) have at least one asymptotic attractor, so that the synchronous solution $\mathbf{s}(t)$, $\mathbf{w}(t)$ is invariant.

S2: Next, we study the local stability of the synchronous solutions (9) and (10), in the presence of small perturbations $\boldsymbol{\delta}\mathbf{x}$ and $\boldsymbol{\delta}\mathbf{y}$, respectively. Thus, we set $\mathbf{s} = \mathbf{x}_i - \boldsymbol{\delta}\mathbf{x}_i$ and $\mathbf{w} = \mathbf{y}_i - \boldsymbol{\delta}\mathbf{y}_i$. It follows from the Taylor series expansion that $\mathbf{f}(\boldsymbol{\delta}\mathbf{x}_i + \mathbf{s}) \approx \mathbf{f}(\mathbf{s}) + D\mathbf{f}(\mathbf{s})\boldsymbol{\delta}\mathbf{x}_i$, with $D\mathbf{f}(\mathbf{s})$ being the time-varying Jacobian matrix of $\mathbf{f}(\cdot)$. Let $\Delta_x := [\boldsymbol{\delta}\mathbf{x}_1^T, \ldots, \boldsymbol{\delta}\mathbf{x}_N^T]$ and $\Delta_y := [\boldsymbol{\delta}\mathbf{y}_1^T, \ldots, \boldsymbol{\delta}\mathbf{y}_N^T]$ be the stack vectors of the perturbed states of the network, we can recast the overall perturbed dynamics about the synchronous solution as

$$\frac{d\Delta_x}{dt} = \left[(\mathbf{I}_N \otimes D\mathbf{f}(\mathbf{s})) - \sigma\alpha(\mathcal{L} \otimes \mathbf{\Gamma}_P)\right]\Delta_x - \sigma\beta(\mathcal{L} \otimes \mathbf{I}_n)\Delta_y, \tag{11}$$

$$\frac{d\Delta_y}{dt} = (\mathbf{I}_N \otimes \mathbf{\Gamma}_I)\Delta_x. \tag{12}$$

S3: Then, a state transformation is considered in order to decouple the perturbation dynamics of any single node from the others. In particular, from the fact that the network is assumed to be undirected and connected (see Assumption II.1), we can eigen-decompose the Laplacian matrix as $\mathcal{L} = \mathbf{Q}\Lambda\mathbf{Q}^T$ with $\mathbf{Q}$ being an appropriate orthonormal matrix. Then, using the state transformation $\boldsymbol{\zeta} := (\mathbf{Q}^{-1} \otimes \mathbf{I}_n)\Delta_x$ and $\boldsymbol{\xi} := (\mathbf{Q}^{-1} \otimes \mathbf{I}_n)\Delta_z$, we can recast equations (11) and (12) in the block-diagonal form as

$$\frac{d\boldsymbol{\zeta}_i}{dt} = [D\mathbf{f}(\mathbf{s}) - \sigma\alpha\lambda_i\mathbf{\Gamma}_P]\boldsymbol{\zeta}_i - \sigma\beta\lambda_i\mathbf{I}_N\boldsymbol{\xi}_i, \tag{13}$$

$$\frac{d\boldsymbol{\xi}_i}{dt} = \mathbf{\Gamma}_I\boldsymbol{\zeta}_i. \tag{14}$$

Note that for $\lambda_1 = 0$, the equations are equal to those of a single uncoupled system, while the other $N-1$ blocks differ from each other by the coupling terms $\sigma\alpha\lambda_k$ and $\sigma\beta\lambda_k$ for $k = \{2, \ldots, N\}$. Therefore, each block of (13) and (14) can be parametrised considering a "master node" equation,[28] by setting $\tilde{\alpha} = \sigma\alpha\lambda_i$ and $\tilde{\beta} = \sigma\beta\lambda_i$, yielding the parametrized equations

$$\frac{d\tilde{\boldsymbol{\zeta}}}{dt} = [D\mathbf{f}(\mathbf{s}) - \tilde{\alpha}\mathbf{\Gamma}_P]\tilde{\boldsymbol{\zeta}} - \tilde{\beta}\tilde{\boldsymbol{\xi}}, \tag{15}$$

$$\frac{d\tilde{\boldsymbol{\xi}}}{dt} = \mathbf{\Gamma}_I\tilde{\boldsymbol{\zeta}}. \tag{16}$$

S4: Finally, the local transversal stability of the synchronous solutions (9) and (10) can be assessed by computing the

Maximum Lyapunov Exponent (MLE) of the variational equations (15) and (16) as a function of the parameters $\tilde{\alpha}$ and $\tilde{\beta}$. We denote this MLE value as $\Psi_I(\tilde{\alpha},\tilde{\beta})$, which we term as the *PI Master Stability Function* (PI-MSF).

It is important to highlight that if the matrix $\mathbf{\Gamma}_I$ has r null rows, then r zero Lyapunov Exponents (LEs) will appear when studying the variational equation (16). Those zero values should not be taken into account when calculating the PI-MSF since they represent non-existing interconnections between the variables of each node. Hence, let Σ_1 be the set of all the LEs denoted by $\tilde{\lambda}_k$ for $k=\{1,\ldots,2n\}$ of the variational equations (15) and (16), and let Σ_2 be the set of all the null LEs, then the PI-MSF can be defined as

$$\Psi_I(\tilde{\alpha},\tilde{\beta}) = \begin{cases} \max_k \tilde{\lambda}_k, \tilde{\lambda} \in \Sigma_1 & m > r, \tilde{\beta} \neq 0 \\ \max_k \tilde{\lambda}_k, \tilde{\lambda} \in \Sigma_1 \backslash \Sigma_2 & \text{otherwise,} \end{cases} \tag{17}$$

where m is the cardinality of Σ_2, i.e., the number of null LE. Note that the positive values of Ψ_I represent unstable modes, i.e., the network does not exhibit a synchronised motion, while the negative values indicate that the network synchronises.

Note that if the synchronous solution $\mathbf{s}(t)$ represents an equilibrium point, then the stability problem becomes equivalent to that of studying the sign of the real part of the dominant eigenvalue of (15) and (16). An example of nonlinear systems with this characteristics are bistable (or multistable) systems, like the unforced Duffing oscillator[18] or the toggle model in synthetic gene regulatory networks.[17] In this case, the solution $\mathbf{s}(t)$ of the nonlinear model can be selected as one of the different equilibrium points exhibited by these systems. Moreover, when considering linear dynamics at nodes, the synchronization problems become equivalent to the consensus problem[8,9] where for the specific case of identical dynamics synchronization is always achieved for any non-negative coupling strength.

Remark III.1. *Analogous to the classic MSF for networks with only static coupling,*[6] *the PI-MSF can also be classified according to how* $\Psi_I(\tilde{\alpha},\tilde{\beta})$ *intersects the zero manifold. Specifically, we can define the following generic types of PI-MSF. Type I: if* $\Psi_I(\tilde{\alpha},\tilde{\beta})$ *is an increasing function (never becomes negative), then synchronisation cannot be attained, no matter the value of the coupling strengths. Type II: the surface* $\Psi_I(\tilde{\alpha},\tilde{\beta})$ *intersects the zero manifold along a single well defined curve in the gain parameter space as shown in Fig. 1(a). In this case, synchronisation is guaranteed for the set of values* $\tilde{\alpha}$ *and* $\tilde{\beta}$ *that do not belong to the set where* $\Psi_I(\tilde{\alpha},\tilde{\beta})$ *is positive. Type III: The intersection between* $\Psi_I(\tilde{\alpha},\tilde{\beta})$ *and the zero-manifold defines a limited or an unlimited region where the PI-MSF is negative (see Fig. 1(b)). In this case, synchronization is attained for the set of values* $\tilde{\alpha}$ *and* $\tilde{\beta}$ *where* $\Psi_I(\tilde{\alpha},\tilde{\beta})$ *remains negative.*

Remark III.2. *We wish to emphasize that the PI-MSF can be extended to the case of directed network structures, by considering that the eigenvalues of* $\mathcal{L}$ *in this scenario are complex variables* $\lambda_i \in \mathbb{C}$ *in (15) and (16). Specifically, by setting* $\lambda_i = \lambda_{Re,i} + \mathbf{i}\lambda_{Im,i}$ *with* $\mathbf{i} := \sqrt{-1}$ *and* $\lambda_{Re,i}, \lambda_{Im,i} \in \mathbb{R}$, *one has that (15) can be written as* $d\tilde{\boldsymbol{\zeta}}/dt = [D\mathbf{f}(\mathbf{s}) - (\tilde{\alpha}_{Re} + \mathbf{i}\tilde{\alpha}_{Im})\mathbf{\Gamma}_P]\tilde{\boldsymbol{\zeta}} - \tilde{\beta}\tilde{\boldsymbol{\xi}}$, *where* $\tilde{\alpha}_{Re} := \sigma\alpha\lambda_{Re,i}$ *and* $\tilde{\alpha}_{Im} := \sigma\alpha\lambda_{Im,i}$. *In this case, the PI-MSF depends on three parameters making more difficult its computation and visualization.*

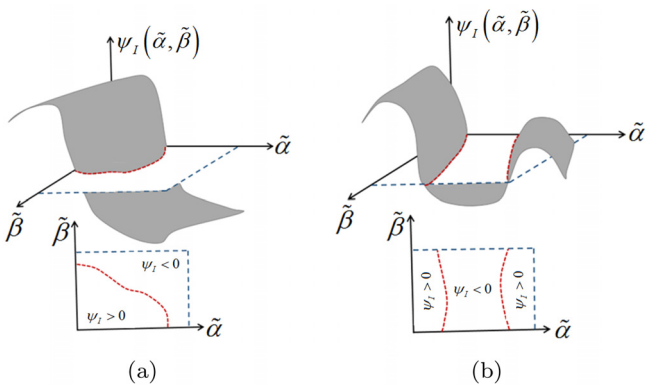

FIG. 1. Generic schematic representation of two possible different scenarios of the MSF for the network (1) with dynamic couplings. The blue dotted-line represents the zero-plane, while the red curve represents the intersection $\Psi_I(\tilde{\alpha},\beta)=0$.

B. MSF for dynamic proportional-derivative coupling

Next, we study the convergence of the network when the proportional and derivative coupling (5) is considered. Letting $\tilde{\mathcal{L}} := \mathbf{I}_{nN} + \sigma\gamma(\mathcal{L}\otimes\mathbf{\Gamma}_D)$, the closed-loop network can be written as

$$\tilde{\mathcal{L}}\left(\frac{d\mathbf{x}}{dt}\right) = \mathbf{F}(\mathbf{x}) - \sigma\alpha(\mathcal{L}\otimes\mathbf{\Gamma}_P)\mathbf{x}, \tag{18}$$

where $\mathbf{F}(\mathbf{x}):=[\mathbf{f}(\mathbf{x}_1)^T,\ldots,\mathbf{f}(\mathbf{x}_N)^T]^T$ and $\mathbf{x}(t):=[\mathbf{x}_1^T(t),\ldots,\mathbf{x}_N^T(t)]^T$ are the stack vectors of the nonlinear functions and node states, respectively. From the fact that the network is undirected (Assumption II.1), one has that $\mathcal{L}=\mathbf{Q}\Lambda\mathbf{Q}^T$, where $\mathbf{Q}\mathbf{Q}^T=\mathbf{I}_N$. Hence, we can write

$$\tilde{\mathcal{L}} = (\mathbf{Q}\mathbf{Q}^T\otimes\mathbf{I}_n) + \sigma\gamma(\mathbf{Q}\Lambda\mathbf{Q}^T\otimes\mathbf{\Gamma}_D),$$

and regrouping terms yields

$$\tilde{\mathcal{L}} = (\mathbf{Q}\otimes\mathbf{I}_n)\tilde{\Lambda}(\mathbf{Q}^T\otimes\mathbf{I}_n), \tag{19}$$

where $\tilde{\Lambda}$ is a diagonal matrix with positive entries given by $\tilde{\Lambda} = \mathbf{I}_{nN} + \sigma\gamma(\Lambda\otimes\mathbf{\Gamma}_D)$.

Note that the entries of the diagonal matrix $\tilde{\Lambda}$ are all positive values and they correspond to the eigenvalues of $\tilde{\mathcal{L}}$; therefore, $\tilde{\mathcal{L}}$ is a non-singular matrix and its inverse exists.[8] Next, from (18) we have

$$\frac{d\mathbf{x}}{dt} = \tilde{\mathcal{L}}^{-1}\mathbf{F}(\mathbf{x}) - \sigma\alpha\tilde{\mathcal{L}}^{-1}(\mathcal{L}\otimes\mathbf{\Gamma}_P)\mathbf{x}. \tag{20}$$

Existence of a synchronous solution can be obtained from (20), by setting $\mathbf{s}=\mathbf{x}_1=\cdots=\mathbf{x}_N$ yielding

$$\frac{d\bar{\mathbf{s}}}{dt} = \tilde{\mathcal{L}}^{-1}(\mathbb{1}_N\otimes\mathbf{f}(\mathbf{s})) - \sigma\alpha\tilde{\mathcal{L}}^{-1}(\mathcal{L}\otimes\mathbf{\Gamma}_P)(\mathbb{1}_N\otimes\mathbf{s}), \tag{21}$$

where $\bar{\mathbf{s}} = (\mathbb{1}_N\otimes\mathbf{s}) = [\mathbf{s}^T,\ldots,\mathbf{s}^T]^T$. Since $\mathcal{L}$ has a zero row-sum, we have that $\mathcal{L}\mathbb{1}_N = \mathbb{0}_{N\times 1}$; hence, the last term of the right-hand side of (21) is null. Moreover, from the definition of $\tilde{\mathcal{L}}$, it is easy to see that $\tilde{\mathcal{L}}(\mathbb{1}_N\otimes\mathbf{f}(\mathbf{s})) = (\mathbb{1}_N\otimes\mathbf{f}(\mathbf{s}))$;

hence, $\tilde{\mathcal{L}}^{-1}(\mathbb{1}_N \otimes \mathbf{f}(\mathbf{s})) = (\mathbb{1}_N \otimes \mathbf{f}(\mathbf{s}))$. Consequently, we have that $d\bar{\mathbf{s}}/dt = (\mathbb{1}_N \otimes \mathbf{f}(\mathbf{s}))$ which corresponds to the equation governing the synchronous motion for each node, which is given by (9). Moreover, letting $\mathbf{P} := \tilde{\mathcal{L}}^{-1}(\mathcal{L} \otimes \mathbf{\Gamma}_D)$ and denoting by $\hat{\mathcal{L}}_{ij}$ and $\mathbf{P}_{ij}$ the $n \times n$ blocks of matrices $\tilde{\mathcal{L}}^{-1}$ and $\mathbf{P}$, respectively, we have

$$\tilde{\mathcal{L}}^{-1} = \begin{bmatrix} \hat{\mathcal{L}}_{11} & \cdots & \hat{\mathcal{L}}_{1N} \\ \vdots & \ddots & \vdots \\ \hat{\mathcal{L}}_{N1} & \cdots & \hat{\mathcal{L}}_{NN} \end{bmatrix}, \quad \mathbf{P} = \begin{bmatrix} \mathbf{P}_{11} & \cdots & \mathbf{P}_{1N} \\ \vdots & \ddots & \vdots \\ \mathbf{P}_{N1} & \cdots & \mathbf{P}_{NN} \end{bmatrix},$$

so that the dynamics of the ith node of network with PD coupling (20) can be written as

$$\frac{d\mathbf{x}_i}{dt} = \sum_{j=1}^{N} \hat{\mathcal{L}}_{ij}\mathbf{f}(\mathbf{x}_j) - \sigma\alpha \sum_{j=1}^{N} \mathbf{P}_{ij}\mathbf{x}_j, \quad \forall i \in \mathcal{N}. \tag{22}$$

Analogous to the case where dynamic PI couplings are considered, here we also follow four steps for assessing the local stability of the synchronous solution (9).

S1: As in the case of Proportional-Integral coupling, we assume the existence of a synchronous invariant trajectory $\mathbf{s}(t)$, which is a solution of the dynamical equations of an isolated node.

S2: Next, we study the stability of the synchronous solution of the closed-loop network (22), in the presence of small perturbations $\boldsymbol{\delta}\mathbf{x}(t)$ whose dynamics are given by

$$\frac{d\boldsymbol{\delta}\mathbf{x}_i}{dt} = \sum_{j=1}^{N} \hat{\mathcal{L}}_{ij} D\mathbf{f}(\mathbf{s})\boldsymbol{\delta}\mathbf{x}_j - \sigma\alpha \sum_{j=1}^{N} \mathbf{P}_{ij}\boldsymbol{\delta}\mathbf{x}_j, \tag{23}$$

which in compact form reads

$$\frac{d\Delta}{dt} = \tilde{\mathcal{L}}^{-1}(\mathbf{I}_N \otimes D\mathbf{f}(\mathbf{s}))\Delta - \sigma\alpha\mathbf{P}\Delta, \tag{24}$$

where $\Delta(t) := [\boldsymbol{\delta}\mathbf{x}_1^T(t), \ldots, \boldsymbol{\delta}\mathbf{x}_N^T(t)]^T$.

S3: From (19), one has that $\tilde{\mathcal{L}}^{-1} = (\mathbf{Q} \otimes \mathbf{I}_n)\tilde{\mathbf{\Lambda}}^{-1}(\mathbf{Q}^T \otimes \mathbf{I}_n)$; therefore,

$$\begin{aligned} \mathbf{P} &= \tilde{\mathcal{L}}^{-1}(\mathcal{L} \otimes \mathbf{\Gamma}_P) \\ &= (\mathbf{Q} \otimes \mathbf{I}_n)\tilde{\mathbf{\Lambda}}^{-1}(\mathbf{\Lambda} \otimes \mathbf{\Gamma}_P)(\mathbf{Q}^T \otimes \mathbf{I}_n). \end{aligned} \tag{25}$$

Hence, applying the state transformation $\boldsymbol{\zeta} = (\mathbf{Q}^T \otimes \mathbf{I}_n)\Delta(t)$ to (24) yields

$$\frac{d\boldsymbol{\zeta}}{dt} = \tilde{\mathbf{\Lambda}}^{-1}\big((\mathbf{I}_N \otimes D\mathbf{f}(\mathbf{s})) - \sigma\alpha(\mathbf{\Lambda} \otimes \mathbf{\Gamma}_P)\big)\boldsymbol{\zeta}. \tag{26}$$

Note that (26) is in the triangular form with N decoupled blocks given by

$$\frac{d\boldsymbol{\zeta}_i}{dt} = (\mathbf{I}_n + \sigma\gamma\lambda_i\mathbf{\Gamma}_D)^{-1}(D\mathbf{f}(\mathbf{s}) - \sigma\alpha\lambda_i\mathbf{\Gamma}_P)\boldsymbol{\zeta}_i. \tag{27}$$

Then, letting $\tilde{\gamma} = \sigma\gamma\lambda_i$ and $\tilde{\alpha} = \sigma\alpha\lambda_i$, we have that the general equation describing the perturbed dynamics of the synchronous state for any node in the network can be written in the parametric form

$$\frac{d\tilde{\boldsymbol{\zeta}}}{dt} = (\mathbf{I}_n + \tilde{\gamma}\mathbf{\Gamma}_D)^{-1}(D\mathbf{f}(\mathbf{s}) - \tilde{\alpha}\mathbf{\Gamma}_P)\tilde{\boldsymbol{\zeta}}. \tag{28}$$

S4: Similar to the PI case, the local stability of the synchronous solution $\mathbf{s}(t)$ can be investigated by computing the MLE, say, $\Psi_D(\alpha, \gamma)$, of the variational equation (28). Hence, synchronisation is guaranteed for the set of values $\tilde{\alpha}$ and $\tilde{\gamma}$ such that $\Psi_D(\tilde{\alpha}, \tilde{\gamma})$ remains negative.

C. Illustrative example

Next, we validate numerically the theoretical derivations of the Master Stability Function for networks with a dynamic diffusive coupling of the PI/PD type.

Consider network (1), where the non-linear vector-field modelling the intrinsic dynamics of each unit is described by the well known Lorenz equation

$$\mathbf{f}(\mathbf{x}) = \begin{bmatrix} \mu(x_2 - x_1) \\ x_1(\rho - x_3) - x_2 \\ x_1x_2 - \omega x_3 \end{bmatrix}, \tag{29}$$

with the parameters set as $\mu = 10, \rho = 28$, and $\omega = 2$ for which the Lorenz system exhibits a chaotic solution.[19]

1. Computation of the PI-MSF

To compute the PI-MSF (17), we start by assuming that the coupling is only through the first state variable, i.e., the inner coupling matrices are set as $\mathbf{\Gamma}_P = \mathbf{\Gamma}_I = \text{diag}\{1, 0, 0\}$. Note that for this particular choice of the inner coupling matrix $\mathbf{\Gamma}_I$, we have that $r = 2$ in (17). We can obtain the synchronous trajectory $\mathbf{s}(t)$ by integrating (9) and (10) with $\mathbf{f}(\cdot)$ being the Lorenz system until it reaches its chaotic attractor.

Next, using the Jacobian matrix of (29) given by

$$D\mathbf{f}(\mathbf{x}) = \begin{bmatrix} -\mu & \mu & 0 \\ \rho - x_3 & -1 & -x_1 \\ x_2 & x_1 & -\omega \end{bmatrix}, \tag{30}$$

we compute the PI-MSF $(\Psi_I(\tilde{\alpha}, \tilde{\beta}))$ by solving the variational equation (15)–(16), using standard methods for estimating the Lyapunov exponents.[37] We then repeat this computation for different values of the parameters $\tilde{\alpha}$ and $\tilde{\beta}$ obtaining the plot shown in Fig. 2(a). For the sake of clarity, we also show the projection of the PI-MSF onto a two dimensional space (see Fig. 2(b)). Here, the positive values of the PI-MSF are colored in a red scale, while the negative values are depicted in blue. Note that pure static coupling ($\beta = 0$) or dynamic coupling ($\alpha = 0$) are both able to guarantee synchronization above a certain threshold. These cases are represented by the red and green curves in Fig. 2. However, both gains can be considerably reduced by using both actions together with a proper tuning. This represents an enhancement of the stability of the synchronous state. Moreover, from Fig. 2(b), we can see that along the line $\tilde{\beta} = 10\tilde{\alpha}$ (white-dashed line in Fig. 2(b)), the Lyapunov exponents decrease almost in a linear manner, suggesting that a faster convergence to synchronization is expected as long as both gains increase. We point out that the

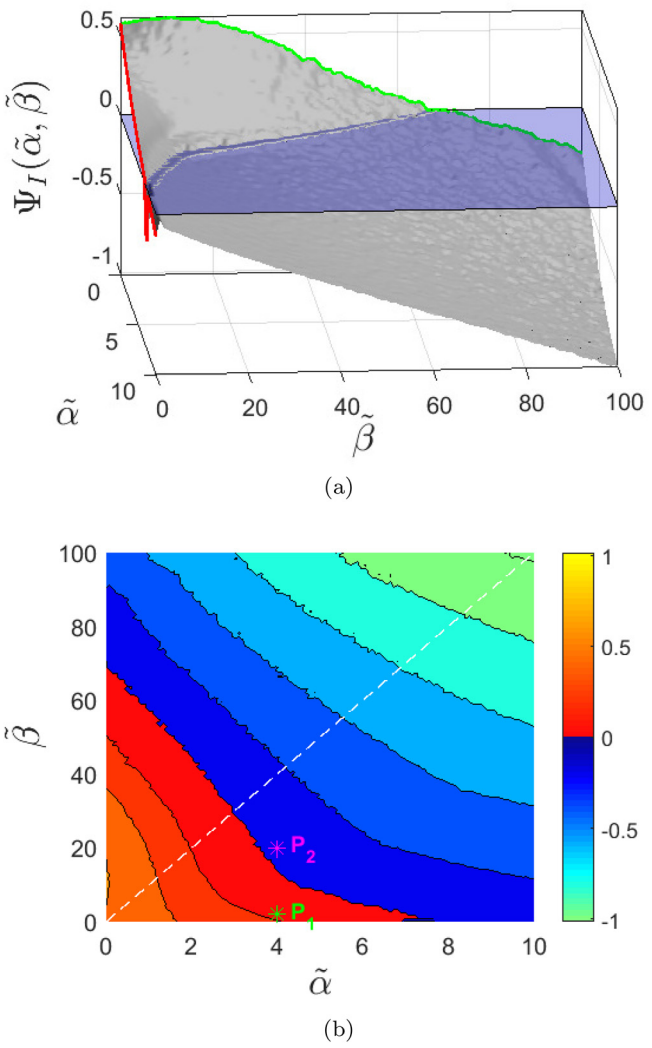

FIG. 2. (a) PI-MSF for chaotic Lorenz with $\Gamma = diag\{1,0,0\}$. The red and light-green curves represent the case when $\beta = 0$ (classic diffusive coupling) and $\alpha = 0$ (purely integral coupling). The blue plane corresponds to $\Psi_I(\tilde{\alpha},\tilde{\beta}) = 0$. (b) Two dimensional representation of the PI-MSF.

enhancement provided by the dynamic PI-coupling can be also exploited for controlling synchronization in networks, by adding extra links such that the PI-MSF becomes negative.[24]

To validate our theoretical predictions for the PI-MSF, we next consider a group of one hundred ($N = 100$) chaotic Lorenz with $\mathbf{\Gamma}_P = \mathbf{\Gamma}_I = \text{diag}\{1,0,0\}$ and three different network configurations: random, scale-free, and small-world as shown in Fig. 3. As a measure of synchronisation, we use the average error dynamics (or disagreement dynamics) given by

$$d(t) := \|\mathbf{x}(t) - (1/N)(\mathbb{1}_N \mathbb{1}_N^T \otimes \mathbf{I}_3)\mathbf{x}(t)\|, \qquad (31)$$

where $d(t) = 0$ indicates that the network has reached synchronisation. We simulate the network at two points in the control parameter space (see Fig. 2(b)). At point $P_1 : (\tilde{\alpha} = 4, \tilde{\beta} = 6)$, where the PI-MSF is positive, and synchronisation should not be attained, and at point $P_2 : (\tilde{\alpha} = 4, \tilde{\beta} = 20)$ where synchronization is ensured. For tuning the proportional α and integral β coupling strengths, we notice that $\tilde{\alpha} = \alpha\sigma\lambda_i$ and $\tilde{\beta} = \beta\sigma\lambda_i$, for any $i \in \mathcal{N}$.

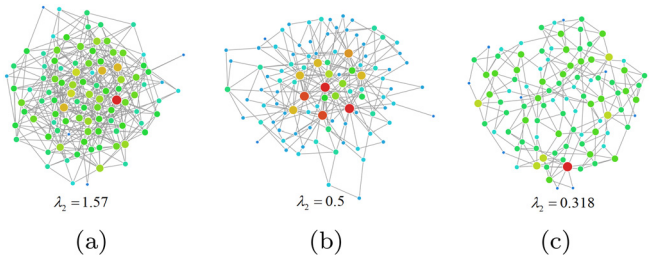

FIG. 3. Three different network structures: (a) random, (b) scale-free, and (c) small world.

Without loss of generality, we set $\sigma = 1$ and explore different network structures setting $\alpha = \tilde{\alpha}/(\sigma\lambda_2)$ and $\beta = \tilde{\beta}/(\sigma\lambda_2)$ at each of the two points (P_1 and P_2) and for each of the network structures being considered. A summary of the gain selection is reported in Table I together with the algebraic connectivity λ_2 of the networks under investigation.

The time responses of the error dynamics $d(t)$ at points P_1 and P_2 for the three network configurations are shown in Figs. 4(a) and 4(b), respectively. As expected, at P_1 no synchronization is attained, while at P_2 the error $d(t)$ asymptotically converges to zero, indicating that all the node states converge toward each other in all the three network configurations.

Note that for the random network, the synchronization error $d(t)$ at P_1 oscillates in a lower range of values than the scale-free and small world, suggesting that a better

TABLE I. Coupling gains for the PI.

Point	Rand. ($\lambda_2 \approx 1.6$)	S.F. ($\lambda_2 \approx 0.5$)	S.W. ($\lambda_2 \approx 0.3$)
$\alpha(P1)$	2.547	8	12.578
$\beta(P1)$	3.821	12	18.867
$\alpha(P2)$	2.547	8	12.578
$\beta(P2)$	12.738	40	62.893

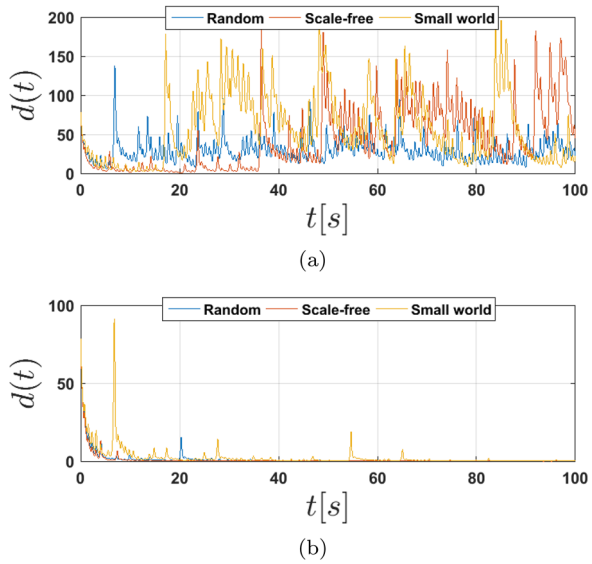

FIG. 4. Evolution of the error dynamics for a network of 100 Lorenz coupled with dynamic PI for three different network topologies: random, scale free, and small-world: (a) at point P_1; (b) at point P_2.

performance is achieved with this particular configuration. This is strongly related to the algebraic connectivity of the network λ_2, which for the random structure is the highest one (see Table I).

2. Computation of the PD-MSF

Following a similar approach to that used to compute the PI-MSF, we now compute the PD-MSF by solving the variational equation (28) with $\mathbf{\Gamma} = \text{diag}\{1,0,0\}$. The PD-MSF together with its two-dimensional representation is depicted in Fig. 5. From the diagrams of Fig. 5, we note that similar to the PI case, a purely static ($\gamma = 0$) or a dynamic ($\alpha = 0$) coupling is found to be able to guarantee synchronization above a certain threshold. Most importantly, we note once again that an appropriate choice of $\tilde{\alpha}$ and $\tilde{\gamma}$ can considerably enhance the stability of the synchronous solution, suggesting that depending on the network structure (via λ_k, for $k \in \{2,\ldots,N\}$), the static (α) and the dynamic (γ) coupling gains can be properly adjusted in order to guarantee synchronization.

In the following, we validate the theoretical predictions of the PD-MSF shown in Fig. 5 by considering the same

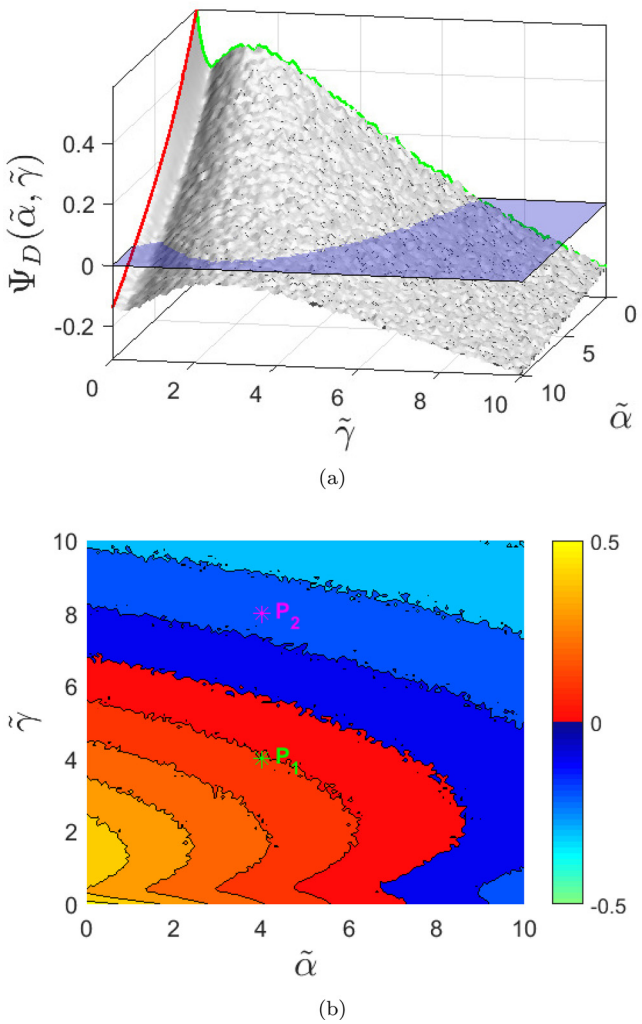

FIG. 5. (a) PD-MSF for chaotic Lorenz with $\mathbf{\Gamma} = diag\{1,0,0\}$. (b) Two dimensional representation of the PD-MSF.

three network structures of the previous example. Note that at the point $P_1 = (\tilde{\alpha},\tilde{\gamma}) = (4,4)$, the networks should not synchronize, while at $P2 = (\tilde{\alpha},\tilde{\gamma}) = (4,8)$ (see diagram in Fig. 5(b)) synchronization should be attained.

Hence, for P_1 we have that $\alpha = \beta$ is equal to 2.54, 7.2, and 12.17 for the random, scale-free, and small world networks, respectively, while for $P_2 : (4,8)$ we have that β is 5.09, 14.41, and 25, 15 for each network configuration. The time response of the three networks at points P_1 and P_2 are shown in Fig. 6 which confirms the theoretical findings.

IV. APPLICATION TO NETWORKS OF MECHANICAL OSCILLATORS

Synchronization in mechanical systems can be traced back to the seventeenth century, to the observation on coupled pendulum clocks made by the Dutch scientist Christiaan Huygens.[32] Nowadays, synchronization in mechanical networks is an active research field with applications including networks of robot manipulators,[27] networks of electromechanical power generators,[15] horizontal platform systems,[1] and harmonic oscillators.[35] Here, we consider a nonlinear oscillator, which is a mass-damper-spring system described by the paradigmatic Duffing equations[31] with an external forcing signal.

A. Mathematical model of the duffing oscillator

The free-body diagram of a duffing oscillator is depicted in Fig. 7, and its dynamics are described by[31]

$$\frac{dx}{dt} = v, \tag{32}$$

$$m\frac{dv}{dt} = -d_y v - \left(-k_y + k_d x^2\right)x + k(F_i - x), \tag{33}$$

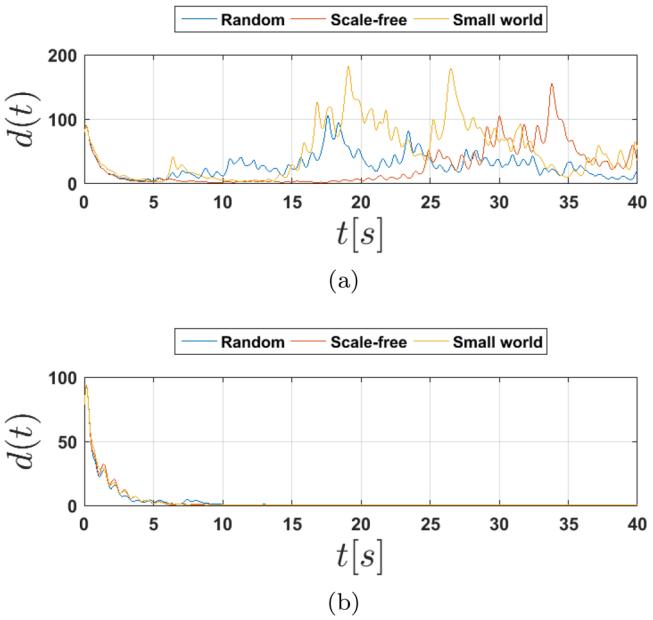

FIG. 6. Evolution of the error dynamics for a network of 100 Lorenz coupled with dynamic PD for the three different network topologies: (a) at point P_1; (b) at point P_2.

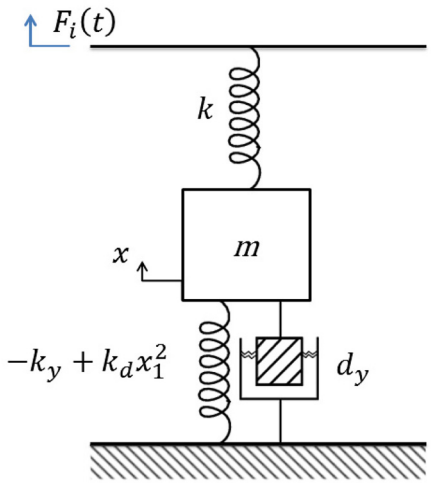

FIG. 7. Free body diagram representation of a nonlinear duffing mechanical oscillator.

where x and v are the position and velocity of a mass m, respectively. d_y is the viscous damping, while k_y and k_d are both constants representing the linear and nonlinear stiffness of the spring, respectively. $F_i(t) := \delta(t) + u_i(t)$ is an external forcing signal which is transmitted through a linear spring with an associated constant stiffness k. $\delta(t)$ is the periodic forcing signal given by $\delta(t) := q\sin(\omega t)$ and u_i is a control input.

B. Mechanical network model

We consider the case where N duffing oscillators can be interconnected through ideal linear springs and dampers with associated constants k_c and d_c, respectively (see Fig. 8). Thus, the mechanical network of duffing oscillators can be represented by a graph $\mathcal{G} = (\mathcal{N}, \mathcal{E})$, where $\mathcal{N}$ is the set of indices for each oscillator and $\boldsymbol{\mathcal{E}}$ denotes the set of interconnections between any pair of Duffing oscillators. The overall network dynamics can then be written as

$$\frac{dx_i}{dt} = v_i, \tag{34}$$

$$m\frac{dv_i}{dt} = -d_y v_i - \left(-k_y + k_d x_i^2\right)x_i + k(\delta(t) - x_i) + ku_i + \sum_{j=1}^{N} a_{ij}\left[k_c(x_j - x_i) + d_c\frac{d}{dt}(x_j - x_i)\right], \tag{35}$$

where x_i and v_i represent the position and velocity of the ith oscillator. a_{ij} are the elements of the adjacency matrix with $a_{ij} = 1$ if there is an interconnection between oscillator i and j and $a_{ij} = 0$ otherwise, for any $i, j \in \mathcal{N}$. Next we show that the mechanical network (34) and (35) can be written as network (1) with dynamic diffusive coupling of PD type, and we study the synchronization of the network when the control action is first absent and then when there is coupling through a feedback on the accelerations of neighbouring oscillators.

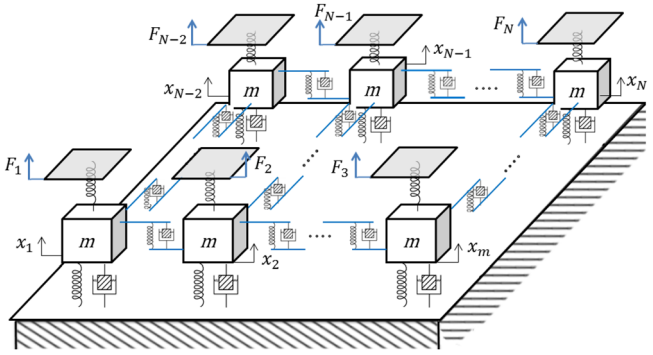

FIG. 8. Network of interconnected mechanical duffing oscillators.

C. Mechanical network neglecting the control input

In this case, we consider $u_i = 0$ in (35) and we assess the stability of the synchronous solutions. Then, by setting $\mathbf{x}_i := [x_i, y_i]^T$, $a = -d_y/m$, $b = (k_y - k)/m$, $c = -k_d/m$, $d = k/m$, the overall network dynamics can be written in compact form (1) with $\sigma = 1/m$, and

$$\mathbf{f} = \begin{bmatrix} v \\ av + bx + cx^3 + d\delta(t) \end{bmatrix}, \tag{36}$$

while the dynamic coupling $\mathbf{h}(\mathbf{x}_j, \mathbf{y}_j)$ is a proportional-derivative one (5) with $\alpha = k_c$, $\gamma = d_c$ and

$$\mathbf{\Gamma}_P = \mathbf{\Gamma}_I = \begin{bmatrix} 0 & 0 \\ 1 & 0 \end{bmatrix}.$$

Note that the first row of the inner coupling matrix is zeros since the first state variable of each oscillator is not affected by any coupling term and feedback is implemented through the second state variable with contributions depending only on the position x_i of the neighbouring duffing systems. We set the parameters of each oscillator as $a = -0.1$, $b = 0$, $c = 1$, $k = 3$, $q = 1.8667$, and $\omega = 1$ so that they exhibit a chaotic behaviour.[19] Also without the loss of generality, we assume all oscillators have unitary mass $m = 1$ so that $\sigma = 1$. Then following a procedure similar to that followed for the Example III C, we obtain the two dimensional diagram of the PD-MSF shown in Fig. 9(a), for the network of Duffing oscillators.

Note that when the oscillators are only coupled through springs, i.e., via purely proportional coupling ($\tilde{\gamma} = 0$), we have that the MSF exhibits multiple intersections at zero, leading to two unstable regions where synchronization is not attained. When a damper is included in the coupling, i.e., an additional derivative action is added to the coupling among oscillators, stability is much improved, as for values of $\tilde{\gamma} > 0.16$ we observe the PD-MSF to be always negative for any value of $\tilde{\alpha}$.

D. Mechanical network with distributed acceleration control

Next we use our theoretical derivations to design a distributed control action to extend the network synchronizability region. Specifically, we consider the following coupling protocol based on the accelerations of the oscillators in the network. Namely, we set

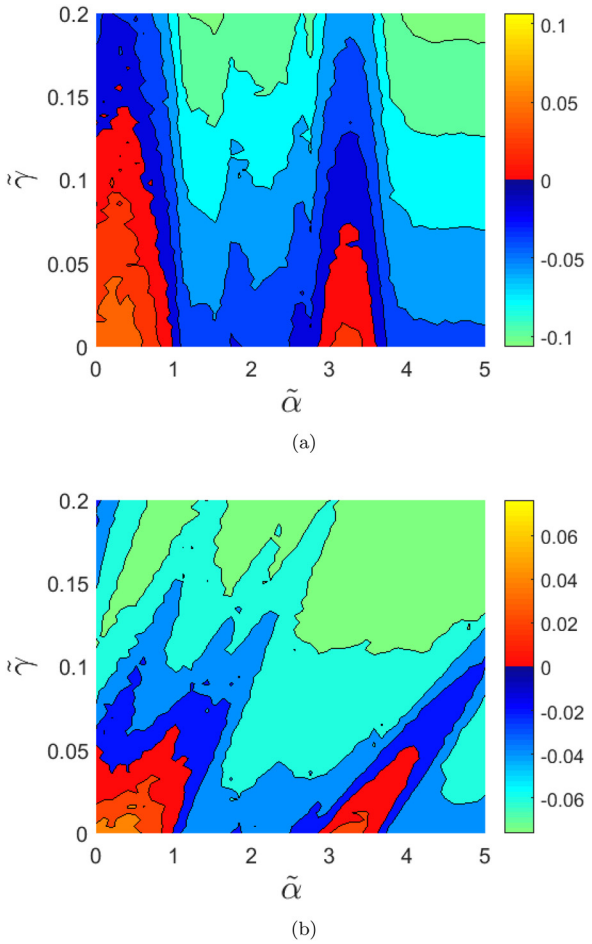

FIG. 9. Two dimensional representation of the PD-MSF, for networks of Duffing oscillators with (a) null control input $u_i, i = \{1, \ldots, N\}$, and (b) distributed acceleration control (37) with $K_u = 2$.

$$u_i = K_u \frac{d_c}{k} \sum_{j=1}^{N} a_{ij} \left(\frac{dv_j}{dt} - \frac{dv_i}{dt} \right), \tag{37}$$

where dv_i/dt is the acceleration of the ith oscillator and K_u is the control gain. Using the notation introduced above, we can rewrite the resulting network as a network of the form (1) coupled through the PD protocol in (5) with

$$\mathbf{\Gamma}_P = \begin{bmatrix} 0 & 0 \\ 1 & 0 \end{bmatrix}, \quad \mathbf{\Gamma}_I = \begin{bmatrix} 0 & 0 \\ 1 & K_u \end{bmatrix}.$$

Solving the variational equation (28), we obtain the two dimensional diagram shown in Fig. 9(b) when $K_u = 2$. Note that the new coupling strategy notably extends the stability region when compared to Fig. 9(a). In particular, we now observe the PD-MSF to remain negative for any value of $\tilde{\alpha}$ when $\tilde{\gamma}$ is greater than 0.05.

Contrary to the case where no control action is present and the coupling matrices are set to be identical $\mathbf{\Gamma}_P = \mathbf{\Gamma}_I$, the addition of the feedback control term (37) makes the coupling matrices $\mathbf{\Gamma}_P$ and $\mathbf{\Gamma}_I$ to be different from each other. Such independence of the coupling matrices has a notably effect on the stability by expanding the region where synchronization is attained. Even recent studies on this aspect[39] support the idea that this independence on the inner coupling matrices represents an extra degree of freedom that may be used to enhance synchronization.

We wish to emphasize that the uncontrolled network of mechanical oscillators can be also studied with the classic MSF approach by considering only diffusive static couplings;[31] nevertheless, when the acceleration feedback is present, the overall network dynamics cannot be recast as a static problem and a PD coupling should be considered instead.

V. ROBUSTNESS ASSESSMENT: HETEROGENEOUS NODE DYNAMICS

In many practical applications, networks are often heterogeneous with nodes being described by different vector fields. Therefore, we investigate next synchronization of networks with dynamic PI/PD couplings when a mismatch on the parameters of each node dynamics is present. In particular, we consider a network of the form

$$\frac{d\mathbf{x}_i}{dt} = \mathbf{f}(\mathbf{x}_i, \mu_i) - \sigma \sum_{j=1}^{N} \mathcal{L}_{ij} \mathbf{h}(\mathbf{x}_j, \mathbf{y}_j), \quad \forall i \in \mathcal{N}, \tag{38}$$

where μ_i represents a generic constant parameter. Note that μ_i renders the node dynamics heterogeneous when at least one parameter μ_i of the ith node is different from the others. In this case, exact synchronization cannot be achieved since the nodes do not share a common solution onto which to synchronize. Instead, trajectories remain asymptotically close to each other with a bounded error depending on the coupling strength value and the network structure.[43]

A. Case study I: Nonidentical Lorenz oscillators

For the sake of simplicity, we consider four chaotic Lorenz (29) coupled in an All-to-All network configuration. We set $\mu_i = \omega_i$ as the parameter undergoing mismatches so that $\mu_i = -2$ for $i = 1, 3$ (just nodes 1 and 3), while $\mu_i = -2.15$ otherwise. As a measure of synchronization and to better expound the results of our analysis, we first average the disagreement signal $d(t)$ defined in (31) neglecting the transient response. We denote such average as $\langle d \rangle$. Next we rescale $\langle d \rangle$ in the range of [0, 1] by considering an exponential function

$$\tilde{d} := e^{-c\langle d \rangle}, \tag{39}$$

where c is a non-negative constant representing the sensitivity of the rescaling. Note that for large values of $\langle d \rangle$, $\tilde{d}$ takes values close to zero (high synchronization error), while if instead $\langle d \rangle$ is close to zero, the function $\tilde{d}$ tends to one (corresponding to a lower synchronization error).

We calculate $\tilde{d}$ varying the static coupling gain in the range $\alpha \in [0, 15]$ with an increment step of 0.125 for different values of the integral and derivative coupling strengths. The results are shown in Fig. 10 where for each point we calculate the average of $\tilde{d}$ over 100 trials starting from random initial conditions.

It is important to highlight that for tuning the value of the sensitivity c, the worst case scenario is considered,

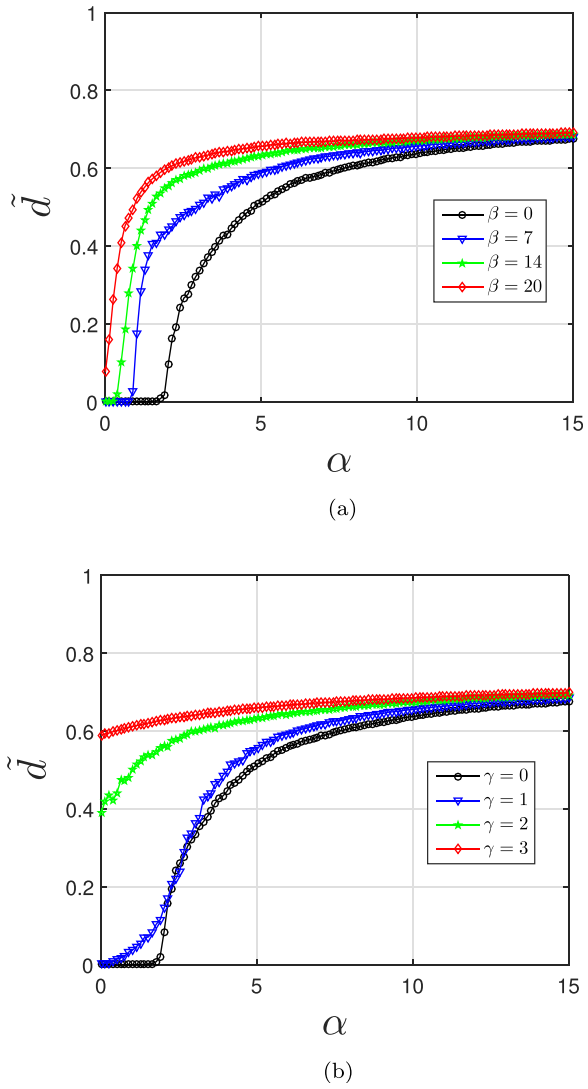

FIG. 10. Rescaled average disagreement with $c = 0.5459$ of an all-to-all network of four chaotic Lorenz coupled via (a) PI and (b) PD couplings.

i.e., all the oscillators are uncoupled. First, note that simplifying c from (39) one has that $c = -ln(\tilde{d})/\langle d \rangle$ with $\tilde{d}$ representing the level of synchronization. Since the oscillators are uncoupled, no synchronization is attained and $\tilde{d}$ should be exactly zero; however, in our numerical simulator, we assume $\tilde{d} = 10^{-5}$ for this worst case scenario. Finally, we calculate $\langle d \rangle$ for 100 different initial conditions yielding $c = -ln(10^{-5})/min_k(\langle d \rangle)$, where $min_k(\langle d \rangle)$ is the best error case out of the $k = 100$ trials, yielding $c = 0.5459$. Note from Fig. 10 that when the integral or derivative actions are neglected (purely proportional diffusive coupling), the network exhibits a smooth transition towards synchronization, and for values of $\alpha > 10$, the normalized synchronization index $\tilde{d}$ is greater than 0.6. If instead an integral/derivative action is considered, the synchronization index can be notably enhanced. Interestingly, by increasing the strength of the dynamic I or D couplings, the transition exhibited by the static case becomes faster; therefore, lower synchronization errors are expected even for low values of the proportional gain $\alpha < 10$, despite the presence of heterogeneities in the nodes. This extra degree of freedom provided by the derivative or the integral gain can be properly used to optimize the network performance, since low values of the coupling strengths may decrease the amount of energy on the links required to achieve bounded synchronization.

B. Case study II: Nonidentical mechanical oscillators

Following the example presented above, we consider again an All-to-All network of four chaotic mechanical oscillators (34) and (35). For the sake of completeness, we first show the case when all the oscillators are identical so that the results of the PD-MSF in Fig. 9(a) are validated. In Fig. 11(a), the rescaled average disagreements $\tilde{d}$ are shown for the All-to-All mechanical network with null control input, using three different values of the derivative gain $\gamma = 0$ (static coupling), $\gamma = 0.0125$, and $\gamma = 0.025$, and $\alpha \in [0, 1.25]$. These values correspond to $\tilde{\gamma} = 0$, $\tilde{\gamma} = 0.05$, and $\tilde{\gamma} = 0.1$, respectively, while $\tilde{\alpha} \in [0, 5]$ ($\lambda_2 = 4$ for an all-to-all network). As expected, synchronization is lost for those gain values where the PD-MSF was predicted to be positive. Moreover, increasing the derivative coupling gain enhances synchronization by increasing the range of values of the proportional gain α where synchronization is attained

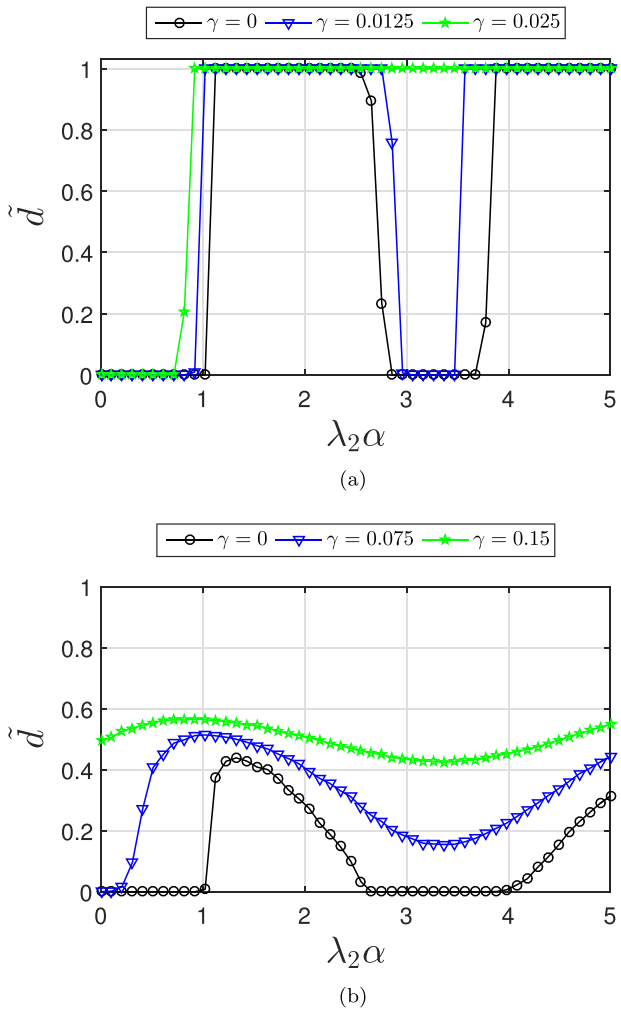

FIG. 11. Rescaled average disagreement for an all-to-all network of four chaotic Duffing oscillators: (a) with identical node dynamics; (b) with heterogeneous node dynamics.

(i.e., $\tilde{d} = 1$). Finally, we choose the amplitude of the forcing signal $\delta(t)$ to be a parameter undergoing mismatches, i.e., $\mu_i = q_i$ for $i = \{1, 2, 3, 4\}$. Specifically, we consider $\mu_i = 1.8667$ for nodes 1 and 3, while $\mu_i = 1.9667$ for nodes 2 and 4, and we calculate the rescaled average disagreement $\tilde{d}$ with $c = 6.1301$ as can be seen in Fig. 11(b). Once again the addition of a derivative term in the coupling among oscillators is shown to improve the network synchronization performance when heterogeneities are present.

VI. CONCLUSIONS

Inspired by a theoretical control approach, we studied two different types of dynamic coupling strategies to achieve synchronization in a network of nonlinear dynamical systems. In both cases, the coupling consists of a static diffusive term complemented by either an integral or a derivative term depending on the mismatch of the states between neighboring nodes. We have shown that the presence of dynamic coupling can notably expand the region where synchronization is attained. The numerical observations were confirmed analytically by extending the well known MSF approach to the case where the couplings are dynamic of PI/PD type. Synchronization regions are shown to be nontrivial functions of the coupling parameters and network structure exhibiting complex geometries. Moreover, we have shown that dynamic couplings are of particular importance when some parameter mismatches are present at nodes, since the coupling gains can be properly tuned for decreasing the residual error. Analytical estimations of such errors are the subject of ongoing work where the aim is to adapt the extended MSF approach[43] to the case of dynamic couplings. We wish to emphasize that the presence of both static and dynamic contributions for each existing link in the network can be relaxed by considering a multiplex approach[9] where the proportional and the integral/derivative couplings are deployed independently from each other. Preliminary numerical results show that this extra-degree of freedom can also be exploited for enhancing synchronization. This is currently under investigation and will be presented elsewhere.

[1]M. P. Aghababa and H. P. Aghababa, "Synchronization of mechanical horizontal platform systems in finite time," Appl. Math. Modell. **36**(10), 4579–4591 (2012).

[2]M. Andreasson, D. V. Dimarogonas, H. Sandberg, and K. H. Johansson, "Distributed control of networked dynamical systems: Static feedback, integral action and consensus," IEEE Trans. Autom. Control **59**(7), 1750–1764 (2014).

[3]M. Bando, K. Hasebe, A. Nakayama, A. Shibata, and Y. Sugiyama, "Dynamical model of traffic congestion and numerical simulation," Phys. Rev. E **51**(2), 1035 (1995).

[4]D. S. Bernstein, *Matrix Mathematics: Theory, Facts, and Formulas*, 2nd ed. (Princeton University Press, 2009).

[5]A. Bidram, F. L. Lewis, and A. Davoudi, "Distributed control systems for small-scale power networks: Using multiagent cooperative control theory," IEEE Control Syst. Mag. **34**(6), 56–77 (2014).

[6]S. Boccaletti, V. Latora, Y. Moreno, M. Chavez, and D. U. Hwang, "Complex networks: Structure and dynamics," Phys. Rep. **424**(4–5), 175–308 (2006).

[7]D. A. Burbano L. and M. di Bernardo, "Consensus and synchronization of complex networks via proportional-integral coupling," in *2014 IEEE International Symposium on Circuits and Systems (ISCAS)* (2014), pp. 1796–1799.

[8]D. A. Burbano L. and M. di Bernardo, "Distributed PID control for consensus of homogeneous and heterogeneous networks," IEEE Trans. Control Network Syst. **2**(2), 154–163 (2015).

[9]D. A. Burbano L. and M. di Bernardo, "Multiplex PI control for consensus in networks of heterogeneous linear agents," Automatica **67**, 310–320 (2016).

[10]R. Carli, A. Chiuso, L. Schenato, and S. Zampieri, "A PI consensus controller for networked clocks synchronization," in *17th IFAC World Congress* (2008), Vol. 17, pp. 10289–10294.

[11]L. Chen, C. Qiu, and H. B. Huang, "Synchronization with on-off coupling: Role of time scales in network dynamics," Phys. Rev. E **79**, 045101 (2009).

[12]L. Cheng, Y. Wang, W. Ren, Z.-G. Hou, and M. Tan, "Containment control of multiagent systems with dynamic leaders based on a PI^n-type approach," IEEE Trans. Cybern. **PP**(99), 1–14 (2015).

[13]M. de Magistris, M. di Bernardo, and C. Petrarca, "Experiments on synchronization in networks of nonlinear oscillators with dynamic links," Nonlinear Theory Appl., IEICE **4**(4), 462–472 (2013).

[14]S. V. Dhople, B. B. Johnson, F. Dörfler, and A. O. Hamadeh, "Synchronization of nonlinear circuits in dynamic electrical networks with general topologies," IEEE Trans. Circuits Syst. I **61**(9), 2677–2690 (2014).

[15]F. Döfler and F. Bullo, "Synchronization in complex networks of phase oscillators: A survey," Automatica **50**(6), 1539–1564 (2014).

[16]R. A. Freeman, P. Yang, and K. M. Lynch, "Stability and convergence properties of dynamic average consensus estimators," in *Proceedings of 45th IEEE Conference on Decision and Control* (2006), pp. 338–343.

[17]T. S. Gardner, C. R. Cantor, and J. J. Collins, "Construction of a genetic toggle switch in *Escherichia coli*," Nature **403**(6767), 339–342 (2000).

[18]P. Holmes, "A nonlinear oscillator with a strange attractor," Philos. Trans. R. Soc. London, Ser. A **292**(1394), 419–448 (1979).

[19]L. Huang, Q. Chen, Y. C. Lai, and L. M. Pecora, "Generic behavior of master-stability functions in coupled nonlinear dynamical systems," Phys. Rev. E **80**, 036204 (2009).

[20]R. Jiang, Q. Wu, and Z. Zhu, "Full velocity difference model for a car-following theory," Phys. Rev. E **64**(1), 017101 (2001).

[21]W. Kinzel, A. Englert, G. Reents, M. Zigzag, and I. Kanter, "Synchronization of networks of chaotic units with time-delayed couplings," Phys. Rev. E **79**, 056207 (2009).

[22]V. Kohar, P. Ji, A. Choudhary, S. Sinha, and J. Kurths, "Synchronization in time-varying networks," Phys. Rev. E **90**, 022812 (2014).

[23]N. E. Leonard, "Multi-agent system dynamics: Bifurcation and behavior of animal groups," Annu. Rev. Control **38**(2), 171–183 (2014).

[24]T. Liu, D. J. Hill, and J. Zhao, "Synchronization of dynamical networks by network control," IEEE Trans. Autom. Control **57**(6), 1574–1580 (2012).

[25]W. Lu and T. Chen, "New approach to synchronization analysis of linearly coupled ordinary differential systems," Physica D **213**(2), 214–230 (2006).

[26]C. Murguia, R. H. B. Fey, and H. Nijmeijer, "Network synchronization using invariant-manifold-based diffusive dynamic couplings with time-delay," Automatica **57**, 34–44 (2015).

[27]H. Nijmeijer and A. Rodriguez-Angeles, "Synchronization of mechanical systems," *World Scientific Series on Nonlinear Science Series A* (World Scientific, 2003) Vol. 46.

[28]L. M. Pecora and T. L. Carroll, "Master stability functions for synchronized coupled systems," Phys. Rev. Lett. **80**, 2109–2112 (1998).

[29]L. M. Pecora and T. L. Carroll, "Synchronization of chaotic systems," Chaos **25**(9), 097611 (2015).

[30]L. M. Pecora, F. Sorrentino, A. M. Hagerstrom, T. E. Murphy, and R. Roy, "Cluster synchronization and isolated desynchronization in complex networks with symmetries," Nat. Commun. **5**, 4079 (2014).

[31]A. Perlikowski and P. Stefanski, "Synchronization of coupled mechanical oscillators," Mech. Mech. Eng. **10**(1), 110–116 (2006).

[32]A. Pikovsky, M. Rosenblum, and J. Kurths, *Synchronization: A Universal Concept in Nonlinear Sciences* (Cambridge University Press, 2001).

[33]G. Popkin, "The physics of life," Nature **529**, 16–18 (2016).

[34]K. J. Åström and T. Hägglund, *PID Controllers - Theory, Design, and Tuning* (International Society for Measurement and Control, 1995).

[35]W. Ren, "Synchronization of coupled harmonic oscillators with local interaction," Automatica **44**(12), 3195–3200 (2008).

[36]M. Righero, F. Corinto, and M. Biey, "Master stability function for networks of chua's circuits with static and dynamic couplings," in *2011 IEEE International Symposium on Circuits and Systems (ISCAS)*, 2011, pp. 737–740.

[37]M. Sandri, "Numerical calculation of Lyapunov exponents," Math. J. **6**(3), 78–84 (1996).
[38]A. Sarlette, J. Dai, Y. Phulpin, and D. Ernst, "Cooperative frequency control with a multi-terminal high-voltage DC network," Automatica **48**(12), 3128–3134 (2012).
[39]R. Sevilla-Escoboza, R. Gutiérrez, G. Huerta-Cuellar, S. Boccaletti, J. Gómez-Gardeñes, A. Arenas, and J. M. Buldú, "Enhancing the stability of the synchronization of multivariable coupled oscillators," Phys. Rev. E **92**, 032804 (2015).
[40]J. W. Simpson-Porco, F. Dörfler, and F. Bullo, "Synchronization and power sharing for droop-controlled inverters in islanded microgrids," Automatica **49**(9), 2603–2611 (2013).
[41]F. Sorrentino, "Synchronization of hypernetworks of coupled dynamical systems," New J. Phys. **14**, 033035 (2012).
[42]S. Strogatz, "Exploring complex networks," Nature **410**, 268–276 (2001).
[43]J. Sun, E. M. Bollt, and T. Nishikawa, "Master stability functions for coupled nearly identical dynamical systems," Europhys. Lett. **85**(6), 60011 (2009).
[44]Y. Tang, F. Qian, H. Gao, and J. Kurths, "Synchronization in complex networks and its applications: A survey of recent advances and challenges," Annu. Rev. Control **38**(2), 184–198 (2014).
[45]P. Wieland, R. Sepulchre, and F. Allögwer, "An internal model principle is necessary and sufficient for linear output synchronization," Automatica **47**(5), 1068–1074 (2011).
[46]P. Wieland, J. Wu, and F. Allögwer, "On synchronous steady states and internal models of diffusively coupled systems," IEEE Trans. Autom. Control **58**(10), 2591–2602 (2013).
[47]Z. Xuan and A. Papachristodoulou, "A distributed PID controller for network congestion control problems," in *American Control Conference (ACC)* (2014), pp. 5453–5458.